Mapping Charge Transport by Electroluminescence in Chirality-Selected Carbon Nanotube Networks

Florian Jakubka,[†] Claudia Backes,[‡,§] Florentina Gannott,[†] Udo Mundloch,[‡] Frank Hauke,[‡] Andreas Hirsch,[‡,⊥] and Jana Zaumseil[†,*]

[†]Institute of Polymer Materials, Friedrich-Alexander-Universität Erlangen-Nürnberg, 91058 Erlangen, Germany, [‡]Institute of Advanced Materials and Processes (ZMP), Friedrich-Alexander-Universität Erlangen-Nürnberg, 90762 Fürth, Germany, [§]School of Physics and CRANN, Trinity College Dublin, Dublin 2, Ireland, and [⊥]Department of Chemistry and Pharmacy, Friedrich-Alexander-Universität Erlangen-Nürnberg, 91054 Erlangen, Germany

ABSTRACT

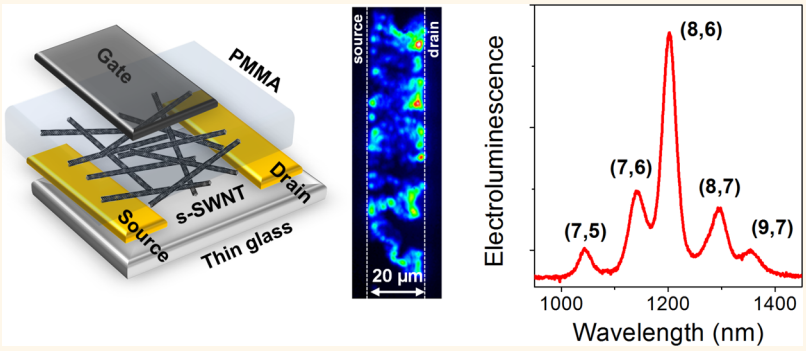

We demonstrate random network single-walled carbon nanotube (SWNT) field-effect transistors (FETs) in bottom contact/top gate geometry with only five different semiconducting nanotube species that were selected by dispersion with poly(9,9-dioctylfluorene) in toluene. These FETs are highly ambipolar with balanced hole and electron mobilities and emit near-infrared light with narrow peak widths (<40 meV) and good efficiency. We spatially resolve the electroluminescence from the channel region during a gate voltage sweep and can thus trace charge transport paths through the SWNT thin film. A shift of emission intensity to large diameter nanotubes and gate-voltage-dependent photoluminescence quenching of the different nanotube species indicates excitation transfer within the network and preferential charge accumulation on small band gap nanotubes. Apart from applications as near-infrared emitters with selectable emission wavelengths and narrow line widths, these devices will help to understand and model charge transport in realistic carbon nanotube networks.

KEYWORDS: single-walled carbon nanotubes · selection · field-effect transistor · electroluminescence · photoluminescence

Near-infrared electroluminescence from semiconducting single-walled carbon nanotubes (s-SWNTs) could be useful for many applications in optoelectronics.[1,2] However, the implementation of s-SWNTs in light-emitting devices has been impeded in the past by their low emission efficiencies and broad spectra.[3,4] Simultaneously, networks of s-SWNTs have attracted much attention as a promising way to obtain high-mobility solution-processed field-effect transistors (FETs).[5−9] Recent advances in the separation of semiconducting and metallic SWNTs have enabled these and other applications in optoelectronic devices. By using density gradient ultracentrifugation,[10] gel chromatography,[11] or selective dispersion in conjugated polymers,[12−15] it is now possible to obtain dispersions with 99% semiconducting nanotubes or even specific chiralities. Random network FETs produced from s-SWNT dispersions exhibit high mobilities as well as high on/off ratios.[5,13,15−18] They can be used in complementary-like inverters for fast ring oscillators[8,19] or as switches in active matrix organic light-emitting diode displays.[7] The use of networks of nanotubes with different diameters and thus different band gaps and mobilities raises the question of how

* Address correspondence to jana.zaumseil@fau.de.

Received for review July 5, 2013 and accepted July 27, 2013.

Published online August 05, 2013
10.1021/nn403419d

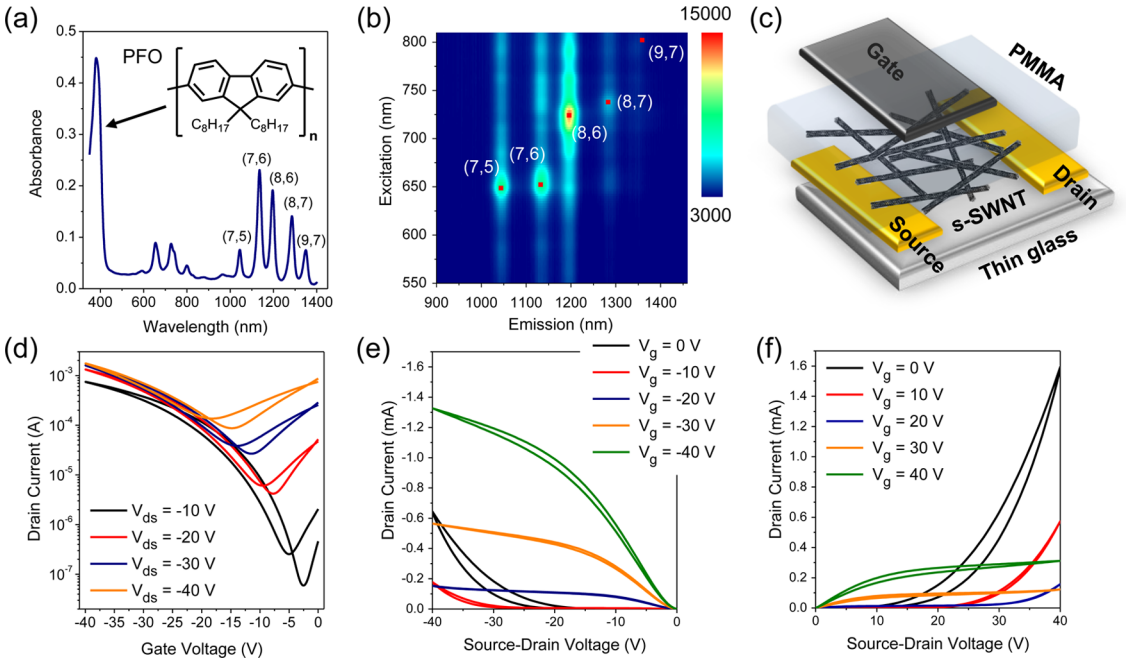

Figure 1. (a) Absorption spectrum of enriched s-SWNT dispersion with minimal residual polymer (PFO, inset). (b) Excitation–emission map of this dispersion showing five dominant nanotube species. (c) Schematic device structure of a bottom contact/top gate FET with selected s-SWNT, PMMA dielectric, and silver gate electrode. (d) Typical ambipolar transfer characteristics of an encapsulated FET with spin-coated s-SWNT. (e,f) Output characteristics of the same device, showing good injection of both holes and electrons and current saturation at high V_{ds}.

current density is distributed within the channel. Previous approaches to model carbon nanotube networks using percolation theory only took into account distributions of metallic and semiconducting nanotubes. Experimental data to validate those models were limited to current–voltage characteristics,[20,21] and thus a detailed understanding is still lacking.

Another intriguing feature of semiconducting carbon nanotubes is their luminescence in the near-infrared that originates from exciton recombination. These excitons can be generated by absorption of light (photoluminescence, PL)[22] or electrically by electron–hole recombination[23] or impact excitation,[24] thus resulting in electroluminescence (EL). Efficient near-infrared light-emitting devices, with selectable emission wavelengths and narrow line widths relying only on carbon-based materials, are highly desirable. The application of devices based on lead chalcogenide nanocrystals[25] will be limited due to health and safety concerns, and other solution-processable near-infrared electroluminescent materials (*e.g.*, rare earth metal complexes[26,27]) are rare or suffer from low efficiency. While PL quantum efficiencies of carbon nanotubes can reach several percent for single free-standing[28] or individualized polymer-wrapped SWNTs,[12] electroluminescent devices (diodes as well as FETs) based on SWNTs as emitters have so far shown poor performance with broadened emission spectra and low quantum efficiencies.[3,4,29,30]

Here we demonstrate ambipolar field-effect transistors based on random networks of only five different semiconducting nanotubes that emit near-infrared light with good efficiency and with the same peak positions and peak widths as their photoluminescence spectra. Tracing the near-infrared emission during a gate voltage sweep allows us to map preferential current paths and thus gain insight into the charge transport in these networks. Gate-voltage-dependent PL quenching indicates the distribution of accumulated holes and electrons in a s-SWNT network depending on the different SWNT band gaps.

RESULTS AND DISCUSSION

To obtain purely semiconducting SWNT thin films, HiPco nanotubes were selectively dispersed in a toluene solution of the conjugated polymer poly(9,9-dioctylfluorene) (PFO).[12,31] After centrifugation, only five semiconducting nanotube species, namely, (7,5), (7,6), (8,6), (8,7), and (9,7), remained in dispersion (Supporting Information Figure S1). The excess polymer was subsequently removed by sedimentation of the nanotubes, washing with toluene, and redispersion of the formed s-SWNT pellet in fresh toluene (see Methods).[18] The absorption spectrum (Figure 1a) and Raman spectra (Supporting Information Figure S2) of the obtained dispersion show no metallic nanotubes and only minimal amounts (<5 μg/mL) of PFO directly associated with the SWNTs. The PL excitation–emission map (Figure 1b) shows a very similar distribution of nanotube species as before sedimentation, with (8,6) as the most abundant chirality. This dispersion was used to form the semiconducting layer by spin-coating

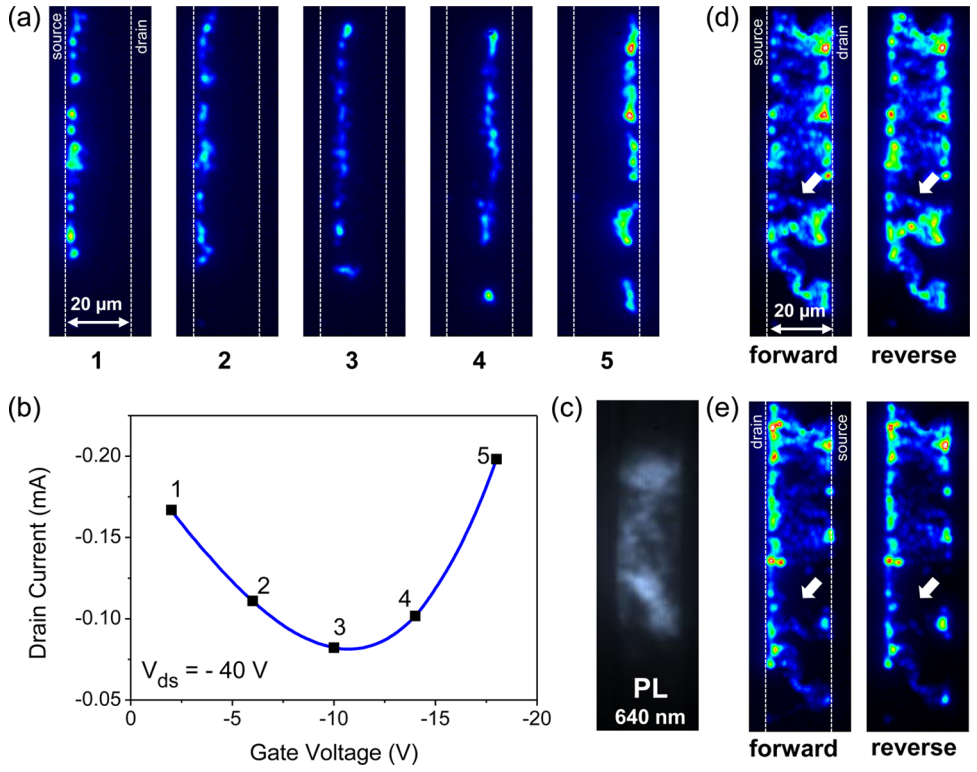

Figure 2. (a) False-color intensity images of near-infrared EL from s-SWNT FET (channel length 20 μm) at different gate voltages and constant source-drain voltage (V_{ds} = −40 V). (b) Current−voltage characteristics for this device during a forward sweep. (c) Photoluminescence image of the channel region excited by a laser diode (640 nm). (d,e) Composite images of EL during forward and reverse gate voltage sweeps visualizing various transport paths through the SWNT film. In one case holes are injected from the left electrode (d), in the other case from the right electrode (e). Note that certain emission paths (white arrow) only show up for hole injection from the left electrode.

or drop-casting onto prepatterned gold electrodes on glass. We used a top-gate FET structure, shown in Figure 1c, with spin-coated PMMA as the gate dielectric and an evaporated silver gate electrode. This device geometry previously proved to be very effective for obtaining ambipolar transport and light emission in a range of conjugated polymers due to improved charge injection assisted by the gate field and elimination of electron traps at the semiconductor−dielectric interface.[31,32] This device geometry also has the additional advantage of being easily encapsulated without degradation, allowing for device operation and characterization in air. The current−voltage characteristics (Figure 1d−f) of the resulting SWNT-FETs are near ideal and show balanced hole and electron transport and little current hysteresis. Charge injection of both carriers appears to be good, although not ohmic. Residual polymer may partially limit injection from the gold into the nanotubes. The saturation field-effect mobilities are estimated to be 0.23 ± 0.17 $cm^2 \cdot V^{-1} \cdot s^{-1}$ for holes and 0.24 ± 0.18 $cm^2 \cdot V^{-1} \cdot s^{-1}$ for electrons using the parallel plate model for the capacitance. Due to the ambipolar nature of these FETs, their on/off current ratios depend strongly on the applied source-drain bias (V_{ds}). For low V_{ds}, the on/off ratio reaches 10^5, which is close to state-of-the-art SWNT network FETs,[5,18] and further corroborates the absence of metallic nanotubes.

In the ambipolar regime of an FET, both holes and electrons are present in the channel and recombination and light emission should take place.[33] The position of the resulting recombination zone is determined by the applied voltages and can be moved from the source electrode through the channel to the drain electrode as was previously demonstrated for ambipolar polymer,[34] single organic crystal,[35] and single carbon nanotube[36] FETs. Here we demonstrate the same behavior for a network of s-SWNTs as shown in Figure 2a. Depending on the applied gate voltage (Figure 2b), many near-infrared emission spots are visible and move through the channel (Supporting Information S3, movie). This controlled movement and the absence of continuous light emission from the contacts indicate that emission predominantly results from electron−hole recombination and not impact excitation, which relies on very high electric fields. Note that the spatial resolution of the emission spots is limited to about 1 μm by the emission wavelength (1000−1400 nm) and the optical setup. After ultrasonication, the nanotubes should be shorter than 1−2 μm, so that any emission spot may originate from a collection of several nanotubes.

In contrast to a uniform polymer film,[37] the emission from the SWNT network is very nonuniform and the emission spots do not move in a straight line from the

source to the drain electrode but sometimes follow tortuous paths. A photoluminescence image (Figure 2c) from the channel area also shows an uneven distribution of emission intensity and thus a nonuniform coverage with SWNTs. A composite image of the electroluminescence (EL) obtained from an entire gate voltage (V_g) sweep reveals the various paths of emission, as shown in Figure 2d for a forward and reverse V_g sweep. The overall image is calculated by assigning to each pixel a color corresponding to the highest brightness value this pixel exhibited during the entire voltage sweep. Interestingly, these composite EL images are not identical with the photoluminescence image of the same area. Clearly, not all nanotubes in the channel contribute to the electroluminescence. As EL can only occur where electrons and holes recombine, the composite EL image shows preferential current paths through the network of nanotubes. Those nanotubes that do not contribute to the charge transport do not appear in the electroluminescence images but are visible in the PL images. The different current pathways probably result from the variation of nanotubes' density, length, band gap, and connectivity within the channel.

Surprisingly, the EL composite images and thus observable current paths also depend on the assignment of the source and drain electrodes, that is, which electrode injects holes or electrons. The differences are mostly subtle, but in some cases, certain EL pathways, as the indicated in Figure 2d,e (white arrow), appear and disappear almost entirely. This effect is reproducible for repeated exchanges of the electrode assignment (see Supporting Information Figure S4a,b). In contrast to that, there is no appreciable difference between images obtained for forward or reverse voltage sweeps, that is, whether the channel changes from hole accumulation to electron accumulation or *vice versa*. This indicates that the observed variations of current paths are likely to arise from preferential injection of holes or electrons depending on energy level alignment and density of different nanotubes at the contacts. Due to the work function of gold (4.8−5 eV), the injection of holes into the network should be favored, but as the band gap of s-SWNTs decreases with increasing diameter, electron injection should increase.

The spatial resolution of the EL maps is quite limited, and in dense films of SWNTs, it cannot distinguish between different nanotubes. However, indirect insight into the charge distribution in networks of different semiconducting SWNTs can be gained from comparing the photoluminescence (excited by a red laser, 640 nm, 5 mW) and electroluminescence spectra from the exact same channel area, as shown in Figure 3. Both spectra exhibit five distinct peaks, which can be fitted with Lorentz profiles with a full width at half-maximum (fwhm) of 25−45 nm (20−37 meV).

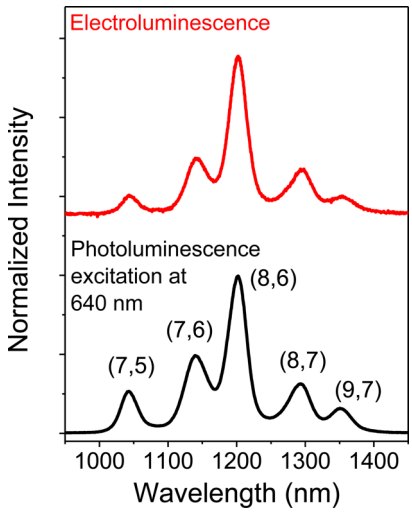

Figure 3. Photoluminescence spectrum (excited at 640 nm, 5 mW, integration time 0.5 s) of s-SWNTs within the channel region and electroluminescence spectrum from the same spot (V_g = 30 V, V_{ds} = 70 V, integration time 60 s).

TABLE 1. Fitted Lorentz Peak Positions, Full Widths at Half-Maximum (fwhm), and Fractions of Overall Intensity for Photoluminescence and Electroluminescence Spectra from the same Spot within the FET Channel

	photoluminescence (excitation 640 nm)			electroluminescence (V_g = 30 V, V_{ds} = 70 V)		
(*n*,*m*)	λ_{center} (nm)	fwhm (nm)	% signal	λ_{center} (nm)	fwhm (nm)	% signal
(7,5)	1043	26	10.3	1044	25	5.3
(7,6)	1140	36	23.9	1141	30	17.7
(8,6)	1201	30	43.2	1202	29	52.8
(8,7)	1292	33	14.8	1294	34	16.6
(9,7)	1353	37	7.8	1357	46	7.6

The different peaks can be ascribed to the five s-SWNT species identified before (see Supporting Information Figure S5 and Table 1). Peak positions and widths do not differ significantly between PL and EL spectra. The obtained PL and EL peak widths are broader than those of PL from single suspended SWNTs (9 meV)[38] but significantly narrower than EL from previous single nanotube and SWNT network devices (80−150 meV),[3,4,39,40] as well as near-infrared PbS nanocrystal light-emitting diodes (100−150 nm).[25] Importantly, there is no severe red shift that is usually observed for EL from single SWNT devices with short channels.[39,40] This is probably due to the relatively low effective lateral fields (2−4 V/μm) in our long channel (20 μm) devices and again supports the notion that excitons are formed by electron−hole recombination and not by impact excitation.

However, the PL spectrum indicates significant energy transfer from the larger band gap nanotubes, that is, (7,5) and (7,6), which are close to resonance with the excitation laser (640 nm), to smaller band gap nanotubes, which are not directly excited at that

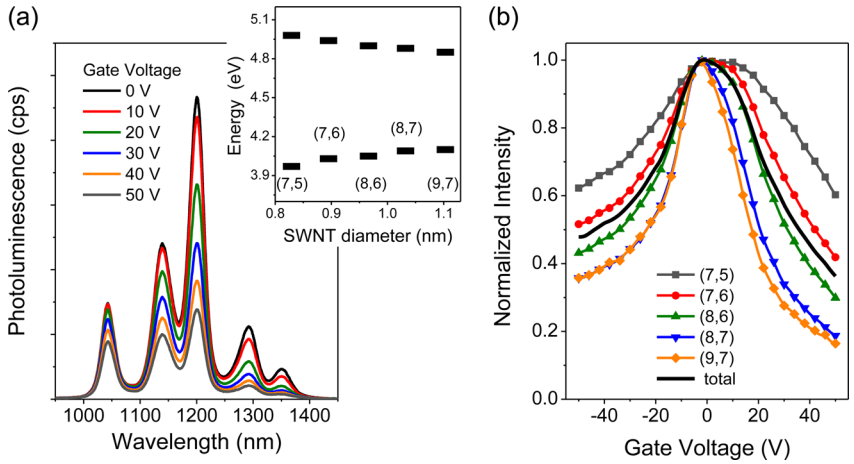

Figure 4. (a) Successive quenching of PL within the FET channel with increasing positive gate voltages (source/drain electrodes grounded). Inset: redox potentials (*i.e.*, energy of first van Hove singularities of the valence and conduction band) for selected SWNTs according to Tanaka *et al.*[50] showing decrease of band gap from (7,5) to (9,7) nanotubes. (b) Normalized peak intensities of corresponding SWNTs and total PL intensity for positive and negative applied gate voltages.

wavelength (see Figure 1b for comparison). The (8,6) nanotube emission is dominant, and the emission from (8,7) and (9,7) nanotubes is much stronger than what would be expected from their population in the dispersion. Clearly, the nanotubes are in intimate contact with each other, and energy transfer can take place. Mehlenbacher *et al.* recently showed that this excitation transfer takes place on a picosecond time scale.[41] The EL spectrum shows even more emission from the smaller band gap nanotubes and from those that are most abundant in the network, that is, the (8,6) SWNTs (Figure 3 and Table 1). Emission from (7,5) and (7,6) nanotubes is strongly diminished compared to the dispersion and also weaker compared to the PL spectrum. Nanotubes with smaller band gaps exhibit higher charge carrier mobilities than those with larger band gaps due to reduced scattering with phonon modes,[42] but more importantly, they are also energetically favorable for both holes and electrons. Predominant charge transfer to and therefore electroluminescence from SWNTs with small band gaps could be expected. Although a quantitative description combining charge transport and excitation transfer is difficult, this notion is supported by the experimental EL spectra.

A preference of charge accumulation on nanotubes with small band gaps is further indicated by the charge carrier density-dependent quenching of photoluminescence from the channel (Figure 4a). Here, different positive and negative gate voltages are applied, while the source and drain electrodes are both grounded and thus charges are accumulated throughout the channel. PL spectra were recorded from a spot in the middle of the channel. While there is no shift in peak position or peak width, the overall PL intensity decreases with positive (accumulation of electrons) and negative (accumulation of holes) gate voltages (Figure 4b). The decrease of emission is not quite linear with gate voltage and thus charge carrier density and not equal for hole and electron accumulation, which may be due to the presence of the polymer. More importantly, the decrease of PL intensity is not uniform, but emission from the small band gap nanotubes declines faster than that of the larger band gap nanotubes, as shown in Figure 4b. The emission from (8,7) and (9,7) SWNTs for V_g = 50 V is quenched to a fifth of the maximum value, while emission from (7,5) SWNTs remains at about two-thirds of its maximum intensity. The reduced PL efficiency of charged SWNTs is generally attributed to an Auger-type E_{11} exciton quenching mechanism.[43] A reduced absorption and hence lower PL due to filling (emptying) of the conduction (valence) band of the SWNTs can be excluded, as this should mainly affect the (7,5) and (7,6) nanotubes, which are in resonance with the excitation laser. These results indicate that accumulated charges in a network of carbon nanotubes are predominantly located on SWNTs with smaller band gaps. In other words, those SWNTs are intrinsic shallow traps for both holes and electrons in a network of s-SWNTs with different diameters (see inset Figure 4a). However, this should not limit the overall mobility as the charge carrier mobility is higher in large diameter nanotubes than in small diameter nanotubes[42] and the SWNT-to-SWNT contact resistance[44] is probably the limiting factor.

Finally, the external quantum efficiency of such a device is crucial for any optoelectronic application. For ambipolar light-emitting FETs, which have narrow movable emission zones, one can assume that all injected charges recombine and form excitons that can relax radiatively or nonradiatively. This leads to very high external quantum efficiencies (EQE) in ambipolar polymer light-emitting FETs.[32,45] The chirality-selected s-SWNTs are wrapped with conjugated polymers, which should increase emission efficiencies compared to the commonly used bare SWNTs.[12] Furthermore, the SWNT films were annealed and

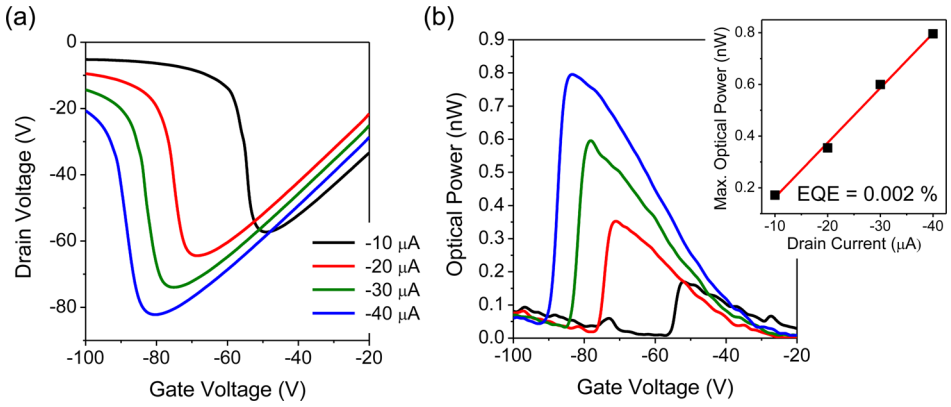

Figure 5. (a) Source-drain voltage *vs* gate voltage plots for fixed constant drain currents of −10 to −40 μA. (b) Near-infrared optical output in the near-infrared (800−1600 nm) during each constant current gate voltage sweep. Inset: Optical output *vs* drain current resulting in average external quantum efficiency of about 0.002%.

encapsulated in a dry nitrogen glovebox, and thus oxygen, which is known to quench emission,[46] was largely excluded and device measurements in air became possible. Note that no visible light emission is observed from the polymer, in contrast to devices based on PFO layers with small amounts of SWNT below the percolation limit, which show efficient blue electroluminescence.[31] This is in agreement with previous reports of excitation transfer from the polymer to the nanotubes.[47] For redispersed PFO/SWNT hybrids, we find reduced blue photoluminescence from the polymer when excited at 380 nm but near-infrared emission from all SWNT species instead (see Supporting Information Figure S6).

Figure 5a,b shows constant drain current measurements of a s-SWNT network FET. The drain current is kept at a certain value, while the gate voltage is swept and the source-drain voltage is adjusted accordingly.[48] The maximum optical power recorded with a calibrated InGaAs photodiode positioned on the glass side of the FET increases linearly with the drain current. From this, we can estimate an EQE of about 0.002%, not taking into account losses by internal absorption and waveguiding. This is in the same range as the best single nanotube light-emitting diodes[2] and FETs[49] and orders of magnitude higher than other SWNT network-based devices.[3,4] Optimizing the wrapping of nanotubes with polymer and thus increasing PL efficiency while maintaining good contacts between the nanotubes for fast charge transport and high currents could further improve the overall near-infrared EL efficiency and brightness.

CONCLUSIONS

In summary, we have demonstrated ambipolar light-emitting FETs based on random networks of only five different types of semiconducting carbon nanotubes. Spatial mapping of the electroluminescence allows us to visualize charge transport paths within the nanotube thin film that clearly depend on the density and connectivity of the nanotubes as well as on the different injection of holes and electrons at the contacts. The obtained electroluminescence spectra show the same peaks as the corresponding photoluminescence spectra of the SWNT network with equal center wavelengths and line widths for each nanotube species. A shift of intensity from small diameter nanotubes with larger band gaps to large diameter nanotubes with smaller band gaps for both PL and EL indicate both excitation transfer and charge transfer within the network. Charge carrier density-dependent photoluminescence quenching suggests that both holes and electrons are predominantly located on small band gap nanotubes in networks of different SWNTs. The efficiency of near-infrared light emission is low but much higher than previous electroluminescent devices based on nanotube networks. Further improvement of the nanotube selection process toward single chiralities and optimization of the polymer wrapping could lead to even more efficient near-infrared emitters with a specific wavelength and narrow line width. Moreover, the obtained information on current paths through and charge distribution in the nanotube thin film could be used to inform and improve advanced theoretical transport models for SWNT network FETs.

METHODS

Selective Dispersion of SWNTs. HiPco single-walled carbon nanotubes (1.5 mg·mL^{-1}, Unidym Inc., batch P2172, diameter 0.8−1.2 nm, <11 wt % iron) were dispersed in 3 mg·mL^{-1} PFO (Aldrich, M_w = 75 kg·mol^{-1}, PD = 3.4) solution in toluene and bath sonicated for 90 min. The resulting dispersion was centrifuged at 60 000*g* for 45 min (Beckman Coulter Avanti J26XP). The supernatant was further ultracentrifuged at 268 000*g* for 30 min to remove any remaining bundles and then at 268 000*g* for 8 h to sediment >80% of all nanotubes. Ultracentrifugation was performed with a Beckman Coulter OptimaMax XP table-top centrifuge with a swinging bucket rotor MLS-50 using thick-walled

polyallomer vials. A pellet was formed at the bottom of the centrifuge vial, which was washed several times with toluene to remove most of the residual free polymer. Redispersing the nanotube pellet in toluene by mild sonication for several minutes yielded a stable dispersion with a similar nanotube composition to the original dispersion. Absorption spectra were recorded with a Varian Cary 6000i UV–vis–NIR spectrometer and PL excitation–emission maps with a Horiba Jobin-Yvon Fluorolog-3 spectrometer with a Symphony-II InGaAs diode array detector. Raman spectra were obtained from drop-cast films on glass using a Renishaw InVia Reflex Raman microscope.

Device Fabrication. Interdigitated source/drain electrodes were patterned on thin glass substrates (Schott AF32 Eco, thickness 700 μm) by photolithography (double-layer photoresist LOR5B/S1813), electron-beam evaporation of 2 nm chromium and 30 nm gold, and lift-off (channel width W = 20 mm, channel length L = 20 μm). The nanotube dispersion was spin-coated onto the substrates at 1000 rpm three times or drop-cast several times, and the resulting films were annealed in a dry nitrogen glovebox at 290 °C for 30 min to remove residual water and oxygen. Spin-coating PMMA (Polymer Source Inc., M_w = 315 kg·mol^{-1}, PD = 1.05) from filtered, anhydrous *n*-butylacetate solution (60 mg·mL^{-1}) on top of the SWNT film formed the dielectric layer (thickness ~700 nm, C_i = 3.14 nF·cm^{-2}. A simple plate capacitor model was used for mobility calculations due to the high SWNT surface coverage). Thermal evaporation of 30 nm of silver through a shadow mask as a gate electrode completed the FETs. After initial testing inside a dry nitrogen glovebox, all devices were encapsulated with an epoxy resin (Rubnor, PX681C/NC) and all of the following measurements were carried out in air. Current–voltage characteristics were measured with an Agilent 4155C semiconductor parameter analyzer and a Keithley 2600 sourcemeter.

Photoluminescence and Electroluminescence Measurements. PL and EL images were recorded with a thermoelectrically cooled 256 × 360 pixel InGaAs camera (Xenics XEVA-CL-TE3, 800–1600 nm), while spectra were obtained with an Acton SpectraPro SP2358 spectrometer (grating 150 lines/mm) and a liquid-nitrogen-cooled InGaAs line camera (PI Acton OMA V:1024 1.7). For photoluminescence measurements, an OBIS 640 nm laser diode (5 mW) (Coherent Europe B.V.) was used and the laser beam was defocused onto the substrate through the collecting near-infrared objective (Olympus LMPL100XIR 100×, NA 0.80 or Olympus LCPLN50XIR 50×, NA 0.65 with correction for glass thickness) to illuminate an area of about 100 μm in diameter. A cold mirror (750 nm) and a long-pass filter (900 nm) were used to reject visible and scattered laser light. For current–voltage–luminance measurements, a calibrated InGaAs photodiode (Thorlabs FGA21-CAL, active area 3.1 mm^2) was placed directly underneath the device (active area ~1.25 mm^2) to collect as much of the emitted light as possible (the silver gate electrode was reflective), and the photocurrent was recorded at 0 V bias. Calculations of the optical power and EQE took the observed electroluminescence spectrum into account. Given the expected losses due to absorption and waveguiding, the obtained EQE is a lower boundary for the overall efficiency.

Conflict of Interest: The authors declare no competing financial interest.

Acknowledgment. This research was funded by the Deutsche Forschungsgemeinschaft (DFG ZA 638/3) and the Alfried Krupp von Bohlen und Halbach-Stiftung. J.Z. also acknowledges general support by the Cluster of Excellence "Engineering of Advanced Materials" (EXC 315). Carbon nanotube research at the ZMP is supported by the Collaborative Research Center SFB 953 "Synthetic Carbon Allotropes". The authors thank the Chair of Electron Devices at the Friedrich-Alexander-Universität Erlangen-Nürnberg for providing additional measurement software.

Supporting Information Available: Absorption spectrum and excitation–emission PL map of HiPco nanotubes dispersed in PFO/toluene before sedimentation, Raman spectra of redispersed nanotubes after sedimentation at different excitation wavelengths, movie of light emission from the FET during a gate voltage sweep, composite EL images for many consecutive gate voltage sweeps and exchanged source-drain electrodes, fitted Lorentz peaks for PL and EL spectra, and emission–excitation maps showing excitation transfer from the polymer to the SWNTs. This material is available free of charge *via* the Internet at http://pubs.acs.org.

REFERENCES AND NOTES

1. Avouris, P.; Freitag, M.; Perebeinos, V. Carbon-Nanotube Photonics and Optoelectronics. *Nat. Photonics* **2008**, *2*, 341–350.
2. Mueller, T.; Kinoshita, M.; Steiner, M.; Perebeinos, V.; Bol, A. A.; Farmer, D. B.; Avouris, P. Efficient Narrow-Band Light Emission from a Single Carbon Nanotube p-n Diode. *Nat. Nanotechnol.* **2009**, *5*, 27–31.
3. Engel, M.; Small, J. P.; Steiner, M.; Freitag, M.; Green, A. A.; Hersam, M. C.; Avouris, P. Thin Film Nanotube Transistors Based on Self-Assembled, Aligned, Semiconducting Carbon Nanotube Arrays. *ACS Nano* **2008**, *2*, 2445–2452.
4. Adam, E.; Aguirre, C. M.; Marty, L.; St-Antoine, B. C.; Meunier, F.; Desjardins, P.; Menard, D.; Martel, R. Electroluminescence from Single-Wall Carbon Nanotube Network Transistors. *Nano Lett.* **2008**, *8*, 2351–2355.
5. Rouhi, N.; Jain, D.; Burke, P. J. High-Performance Semiconducting Nanotube Inks: Progress and Prospects. *ACS Nano* **2011**, *5*, 8471–8487.
6. Sun, D.-M.; Timmermans, M. Y.; Tian, Y.; Nasibulin, A. G.; Kauppinen, E. I.; Kishimoto, S.; Mizutani, T.; Ohno, Y. Flexible High-Performance Carbon Nanotube Integrated Circuits. *Nat. Nanotechnol.* **2011**, *6*, 156–161.
7. Zhang, J.; Fu, Y.; Wang, C.; Chen, P.-C.; Liu, Z.; Wei, W.; Wu, C.; Thompson, M. E.; Zhou, C. Separated Carbon Nanotube Macroelectronics for Active Matrix Organic Light-Emitting Diode Displays. *Nano Lett.* **2011**, *11*, 4852–4858.
8. Ha, M.; Seo, J.-W. T.; Prabhumirashi, P. L.; Zhang, W.; Geier, M. L.; Renn, M. J.; Kim, C. H.; Hersam, M. C.; Frisbie, C. D. Aerosol Jet Printed, Low Voltage, Electrolyte Gated Carbon Nanotube Ring Oscillators with Sub-5 ms Stage Delays. *Nano Lett.* **2013**, *13*, 954–960.
9. Okimoto, H.; Takenobu, T.; Yanagi, K.; Miyata, Y.; Shimotani, H.; Kataura, H.; Iwasa, Y. Tunable Carbon Nanotube Thin-Film Transistors Produced Exclusively *via* Inkjet Printing. *Adv. Mater.* **2010**, *22*, 3981–3986.
10. Arnold, M. S.; Green, A. A.; Hulvat, J. F.; Stupp, S. I.; Hersam, M. C. Sorting Carbon Nanotubes by Electronic Structure Using Density Differentiation. *Nat. Nanotechnol.* **2006**, *1*, 60–65.
11. Liu, H.; Nishide, D.; Tanaka, T.; Kataura, H. Large-Scale Single-Chirality Separation of Single-Wall Carbon Nanotubes by Simple Gel Chromatography. *Nat. Commun.* **2011**, *2*, 309.
12. Nish, A.; Hwang, J. Y.; Doig, J.; Nicholas, R. J. Highly Selective Dispersion of Singlewalled Carbon Nanotubes Using Aromatic Polymers. *Nat. Nanotechnol.* **2007**, *2*, 640–646.
13. Wang, H.; Mei, J.; Liu, P.; Schmidt, K.; Jiménez-Osés, G.; Osuna, S.; Fang, L.; Tassone, C. J.; Zoombelt, A. P.; Sokolov, A. N.; *et al.* Scalable and Selective Dispersion of Semiconducting Arc-Discharged Carbon Nanotubes by Dithiafulvalene/Thiophene Copolymers for Thin Film Transistors. *ACS Nano* **2013**, *7*, 2659–2668.
14. Mistry, K. S.; Larsen, B. A.; Blackburn, J. L. High-Yield Dispersions of Large-Diameter Semiconducting Single-Walled Carbon Nanotubes with Tunable Narrow Chirality Distributions. *ACS Nano* **2013**, *7*, 2231–2239.
15. Gomulya, W.; Costanzo, G. D.; de Carvalho, E. J. F.; Bisri, S. Z.; Derenskyi, V.; Fritsch, M.; Fröhlich, N.; Allard, S.; Gordiichuk, P.; Herrmann, A.; *et al.* Semiconducting Single-Walled Carbon Nanotubes on Demand by Polymer Wrapping. *Adv. Mater.* **2013**, *25*, 2948–2956.
16. Liyanage, L. S.; Lee, H.; Patil, N.; Park, S.; Mitra, S.; Bao, Z.; Wong, H.-S. P. Wafer-Scale Fabrication and Characterization of Thin-Film Transistors with Polythiophene-Sorted Semiconducting Carbon Nanotube Networks. *ACS Nano* **2011**, *6*, 451–458.
17. Lee, H. W.; Yoon, Y.; Park, S.; Oh, J. H.; Hong, S.; Liyanage, L. S.; Wang, H.; Morishita, S.; Patil, N.; Park, Y. J.; *et al.*

Selective Dispersion of High Purity Semiconducting Single-Walled Carbon Nanotubes with Regioregular Poly-(3-alkylthiophene)s. *Nat. Commun.* **2011**, *2*, 541.
18. Bisri, S. Z.; Gao, J.; Derenskyi, V.; Gomulya, W.; Iezhokin, I.; Gordiichuk, P.; Herrmann, A.; Loi, M. A. High Performance Ambipolar Field-Effect Transistor of Random Network Carbon Nanotubes. *Adv. Mater.* **2012**, *24*, 6147–6152.
19. Ha, M.; Xia, Y.; Green, A. A.; Zhang, W.; Renn, M. J.; Kim, C. H.; Hersam, M. C.; Frisbie, C. D. Printed, Sub-3V Digital Circuits on Plastic from Aqueous Carbon Nanotube Inks. *ACS Nano* **2010**, *4*, 4388–4395.
20. Pimparkar, N.; Guo, J.; Alam, M. A. Performance Assessment of Subpercolating Nanobundle Network Thin-Film Transistors by an Analytical Model. *IEEE Trans. Electron Devices* **2007**, *54*, 637–644.
21. Kumar, S.; Murthy, J. Y.; Alam, M. A. Percolating Conduction in Finite Nanotube Networks. *Phys. Rev. Lett.* **2005**, *95*, 066802.
22. O'Connell, M. J.; Bachilo, S. M.; Huffman, C. B.; Moore, V. C.; Strano, M. S.; Haroz, E. H.; Rialon, K. L.; Boul, P. J.; Noon, W. H.; Kittrell, C.; *et al.* Band Gap Fluorescence from Individual Single-Walled Carbon Nanotubes. *Science* **2002**, *297*, 593–596.
23. Misewich, J. A.; Martel, R.; Avouris, P.; Tsang, J. C.; Heinze, S.; Tersoff, J. Electrically Induced Optical Emission from a Carbon Nanotube FET. *Science* **2003**, *300*, 783–786.
24. Chen, J.; Perebeinos, V.; Freitag, M.; Tsang, J.; Fu, Q.; Liu, J.; Avouris, P. Bright Infrared Emission from Electrically Induced Excitons in Carbon Nanotubes. *Science* **2005**, *310*, 1171–1174.
25. Sun, L.; Choi, J. J.; Stachnik, D.; Bartnik, A. C.; Hyun, B.-R.; Malliaras, G. G.; Hanrath, T.; Wise, F. W. Bright Infrared Quantum-Dot Light-Emitting Diodes through Inter-Dot Spacing Control. *Nat. Nanotechnol.* **2012**, *7*, 369–373.
26. Katkova, M. A.; Bochkarev, M. N. New Trends in Design of Electroluminescent Rare Earth Metallo-Complexes for Oleds. *Dalton Trans.* **2010**, *39*, 6599–6612.
27. Katkova, M. A.; Pushkarev, A. P.; Balashova, T. V.; Konev, A. N.; Fukin, G. K.; Ketkov, S. Y.; Bochkarev, M. N. Near-Infrared Electroluminescent Lanthanide [Pr(III), Nd(III), Ho(III), Er(III), Tm(III), and Yb(III)] N,O-Chelated Complexes for Organic Light-Emitting Devices. *J. Mater. Chem.* **2011**, *21*, 16611–16620.
28. Lefebvre, J.; Austing, D. G.; Bond, J.; Finnie, P. Photoluminescence Imaging of Suspended Single-Walled Carbon Nanotubes. *Nano Lett.* **2006**, *6*, 1603–1608.
29. Perebeinos, V.; Avouris, P. Phonon and Electronic Nonradiative Decay Mechanisms of Excitons in Carbon Nanotubes. *Phys. Rev. Lett.* **2008**, *101*, 057401.
30. Zaumseil, J.; Ho, X. N.; Guest, J. R.; Wiederrecht, G. P.; Rogers, J. A. Electroluminescence from Electrolyte-Gated Carbon Nanotube Field-Effect Transistors. *ACS Nano* **2009**, *3*, 2225–2234.
31. Gwinner, M. C.; Jakubka, F.; Gannott, F.; Sirringhaus, H.; Zaumseil, J. Enhanced Ambipolar Charge Injection with Semiconducting Polymer/Carbon Nanotube Thin Films for Light-Emitting Transistors. *ACS Nano* **2012**, *6*, 539–548.
32. Zaumseil, J.; McNeill, C. R.; Bird, M.; Smith, D. L.; Ruden, P. P.; Roberts, M.; McKiernan, M. J.; Friend, R. H.; Sirringhaus, H. Quantum Efficiency of Ambipolar Light-Emitting Polymer Field-Effect Transistors. *J. Appl. Phys.* **2008**, *103*, 064517.
33. Zaumseil, J.; Sirringhaus, H. Electron and Ambipolar Transport in Organic Field-Effect Transistors. *Chem. Rev.* **2007**, *107*, 1296–1323.
34. Zaumseil, J.; Donley, C. L.; Kim, J. S.; Friend, R. H.; Sirringhaus, H. Efficient Top-Gate, Ambipolar, Light-Emitting Field-Effect Transistors Based on a Green-Light-Emitting Polyfluorene. *Adv. Mater.* **2006**, *18*, 2708–2712.
35. Takahashi, T.; Takenobu, T.; Takeya, J.; Iwasa, Y. Ambipolar Light-Emitting Transistors of a Tetracene Single Crystal. *Adv. Funct. Mater.* **2007**, *17*, 1623–1628.
36. Tersoff, J.; Freitag, M.; Tsang, J. C.; Avouris, P. Device Modeling of Long-Channel Nanotube Electro-Optical Emitter. *Appl. Phys. Lett.* **2005**, *86*, 263108.
37. Zaumseil, J.; Kline, R. J.; Sirringhaus, H. Electroluminescence Imaging and Microstructure of Organic Light-Emitting Field-Effect Transistors. *Appl. Phys. Lett.* **2008**, *92*, 073304.
38. Lefebvre, J.; Fraser, J. M.; Finnie, P.; Homma, Y. Photoluminescence from an Individual Single-Walled Carbon Nanotube. *Phys. Rev. B* **2004**, *69*, 075403.
39. Xia, F. N.; Steiner, M.; Lin, Y. M.; Avouris, P. A Microcavity-Controlled, Current-Driven, On-Chip Nanotube Emitter at Infrared Wavelengths. *Nat. Nanotechnol.* **2008**, *3*, 609–613.
40. Pfeiffer, M. H. P.; Stürzl, N.; Marquardt, C. W.; Engel, M.; Dehm, S.; Hennrich, F.; Kappes, M. M.; Lemmer, U.; Krupke, R. Electroluminescence from Chirality-Sorted (9,7)-Semiconducting Carbon Nanotube Devices. *Opt. Express* **2011**, *19*, A1184–A1189.
41. Mehlenbacher, R. D.; Wu, M.-Y.; Grechko, M.; Laaser, J. E.; Arnold, M. S.; Zanni, M. T. Photoexcitation Dynamics of Coupled Semiconducting Carbon Nanotube Thin Films. *Nano Lett.* **2013**, *13*, 1495–1501.
42. Zhou, X. J.; Park, J. Y.; Huang, S. M.; Liu, J.; McEuen, P. L. Band Structure, Phonon Scattering, and the Performance Limit of Single-Walled Carbon Nanotube Transistors. *Phys. Rev. Lett.* **2005**, *95*, 146805.
43. Steiner, M.; Freitag, M.; Perebeinos, V.; Naumov, A.; Small, J. P.; Bol, A. A.; Avouris, P. Gate-Variable Light Absorption and Emission in a Semiconducting Carbon Nanotube. *Nano Lett.* **2009**, *9*, 3477–3481.
44. Znidarsic, A.; Kaskela, A.; Laiho, P.; Gaberscek, M.; Ohno, Y.; Nasibulin, A. G.; Kauppinen, E. I.; Hassanien, A. Spatially Resolved Transport Properties of Pristine and Doped Single-Walled Carbon Nanotube Networks. *J. Phys. Chem. C* **2013**, *117*, 13324–13330.
45. Gwinner, M. C.; Kabra, D.; Roberts, M.; Brenner, T. J. K.; Wallikewitz, B. H.; McNeill, C. R.; Friend, R. H.; Sirringhaus, H. Highly Efficient Single-Layer Polymer Ambipolar Light-Emitting Field-Effect Transistors. *Adv. Mater.* **2012**, *24*, 2728–2734.
46. Lee, A. J.; Wang, X.; Carlson, L. J.; Smyder, J. A.; Loesch, B.; Tu, X.; Zheng, M.; Krauss, T. D. Bright Fluorescence from Individual Single-Walled Carbon Nanotubes. *Nano Lett.* **2011**, *11*, 1636–1640.
47. Nish, A.; Hwang, J. Y.; Doig, J.; Nicholas, R. J. Direct Spectroscopic Evidence of Energy Transfer from Photo-Excited Semiconducting Polymers to Single-Walled Carbon Nanotubes. *Nanotechnology* **2008**, *19*, 095603.
48. Freitag, M.; Chen, J.; Tersoff, J.; Tsang, J. C.; Fu, Q.; Liu, J.; Avouris, P. Mobile Ambipolar Domain in Carbon-Nanotube Infrared Emitters. *Phys. Rev. Lett.* **2004**, *93*, 076803.
49. Freitag, M.; Perebeinos, V.; Chen, J.; Stein, A.; Tsang, J. C.; Misewich, J. A.; Martel, R.; Avouris, P. Hot Carrier Electroluminescence from a Single Carbon Nanotube. *Nano Lett.* **2004**, *4*, 1063–1066.
50. Tanaka, Y.; Hirana, Y.; Niidome, Y.; Kato, K.; Saito, S.; Nakashima, N. Experimentally Determined Redox Potentials of Individual (*n*,*m*) Single-Walled Carbon Nanotubes. *Angew. Chem., Int. Ed.* **2009**, *48*, 7655–7659.